Microstructure - acoustic properties relationships: Application to membrane and bimodal pore-size distribution effects

Camille Perrot, M. T. Hoang, Guy Bonnet, F. Chevillotte, F.-X. Bécot, L. Jaouen, Laurent Gautron, R. Combes, A. Duval, J.-F. Rondeau

Microstructure □ acoustic properties relationships: Application to membrane and bimodal pore-size distribution effects

C. Perrot[1], M. T. Hoang[1], G. Bonnet[1], F. Chevillotte[2], F.-X. Bécot[3], L. Jaouen[3], L. Gautron[4], R. Combes[4], A. Duval[5], J.-F. Rondeau[5]

[1] Université Paris-Est, Laboratoire Modélisation et Simulation Multi Echelle, MSME UMR 8208 CNRS
5 bd Descartes, 77454 Marne-la-Vallée, France
email: **camille.perrot@univ-paris-est.fr**

[2] Fabien Chevillotte
40 B Boulevard Eugène Réguillon, 69100 Villeurbanne, France

[3] Matelys - Acoustique & Vibrations
20/24 rue Robert Desnos, 69120 Vaulx-en-Velin, France

[4] Université Paris-Est, Laboratoire Géomatériaux et Géologie de l'Ingénieur, G2I EA 4119 CNRS
5 bd Descartes, 77454 Marne-la-Vallée, France

[5] Faurecia Acoustics and Soft Trim Division, R&D Center
Route de Villemontry, Z.I. BP13, 08210 Mouzon, France

Abstract

This paper presents recent developments in the field of multi-scale acoustics of real porous media. The fundamental idea of the proposed approach is that it is possible to get insight into the microstructure of real porous media and how it collectively dictates their acoustical properties, from the three-dimensional implementation of micro-acoustics based scaling relations on idealized unit-cells. The homogenization procedure is applied to the problem of long-wavelength wave propagation in rigid porous media saturated with a visco-thermal fluid. The local problems corresponding to the fluid phase have been solved for the three-dimensional tetrakaidecahedronal model. The geometry of the foam is determined based on two measured macroscopic parameters: 1) the porosity and 2) the hydraulic permeability. The complete set of transport phenomena characterizing the asymptotic behavior of the frequency dependant viscous and thermal dissipation functions are systematically determined. The results of this technique are compared to standing wave tube and micrograph measurements for three real samples of predominately open-celled foams. Membrane and bimodal pore-size distribution effects are identified from this comparison.

1 Introduction

The local scale geometry determination of the acoustical properties which characterize the macro behavior of porous media is a long-standing problem of great interest [1]-[3], for instance for the oil, automotive, and aeronautic industries. Various methods have been proposed to solve it on a rigorous basis.

The first problem consists in the idealization at the local scale of real media. For example open-celled foams can be idealized as regular arrays of polyhedrons. A presentation of various idealized shapes is given by Gibson and Ashby [4] for cellular solids, and more specifically by Weaire and Hutzler [5] for foams.

The second problem consists in the determination of the macroscopic and frequency-dependant transport properties, such as the dynamic viscous permeability [6]. The number of media which can be analytically addressed is deceptively small [7], and many techniques have been developed in the literature, such as the self consistent method providing mean estimates (see, for instance, the recent work of Boutin and Geindreau and references therein [8]).

The purpose of this paper is to present a technique based on first-principles calculations of transport parameters [9] in reconstructed porous media [10] which can be applied to model the acoustic properties of real foam samples predominately open-celled; and to compare its predictions to multi-scale experimental data. The main difficulty in modeling the frequency-dependent viscous and thermal dissipation functions through open-celled foams lies in accurately determining micro-structural characteristics, and how they collectively dictate the acoustical macro-behavior. Since the variability in the foam microstructures makes it very difficult to establish and apply local geometry models to study the acoustics of these foams, an inverse model is proposed to quantitatively grasp the complex internal structure of predominately open-celled foam samples. This is achieved from the standpoint of an idealized periodic unit cell (PUC), whose characteristic lengths are directly deduced with routinely available porosity and hydraulic permeability measurements.

The paper is divided into three sections. The method for linking idealized three-dimensional micro-structures and macro-acoustic properties of open-cell foams is dealt with in Section 2. A generation of three-dimensional idealized periodic unit cells of real foam samples predominately open-celled is presented, together with a computational technique in reconstructed unit-cells of the macroscopic properties of sound absorbing materials. In Section 3, results at micro- and macro- scales are compared with experimental data obtained from optical microscopy and standing wave tube measurements and discussed. The fourth Section is devoted to some concluding remarks which summarize the progress recently made.

2 Micro-structure and macro-acoustic properties of predominately open-celled foams

Only packing of identical isotropic polyhedrons was investigated in the current work. Tetrakaidecahedrons with ligaments of circular cross section shapes with a spherical node at their intersections were considered [11]. They are usually defined from the basis of truncated octahedrons, with ligament lengths L and thicknesses $2r$. A tetrakaidecahedron is a 14-sided polyhedron, with six squares faces and eight hexagonal faces. The average number of edges per face, another polyhedron shape indicator, is equal to $(6\times4 + 8\times6) / 14 \approx 5.14$. The cells have characteristic size D equal to $(2\sqrt{2})L$, between two parallel square faces, of one unit. All subsequent calculations are performed in a cubic sample of volume D^3. The ligaments length L is generally taken much larger than the ligaments thickness $2r$. An example of tetrakaidecahedron for such packings is given in Figure 1.

The simplest macroscopic parameter characterizing the packing geometry is its porosity, or air volume fraction Φ. The porosities of these packed polyhedron samples might be expressed as a function of the inverse of the ligaments elongation $L/2r$,

$$\Phi = 1 - \left(\frac{3\sqrt{2}\pi}{16}\right)\left(\frac{2r}{L}\right)^2 - \left(\frac{\sqrt{2}\pi D_1}{16}\right)\left(\frac{2r}{L}\right)^3, \qquad (1)$$

with $D_1 = f^3 - (f^2-1)(3f - \sqrt{f^2-1})$, and f is a spherical node size parameter such that $R = f \times r$, and $f \geq \sqrt{2}$. This last constraint on the node parameter ensures that the exposed surface area at the node is positive and the node volume is larger than the volume of the connecting ligaments at the node, assuming a lump of material at ligament intersection.

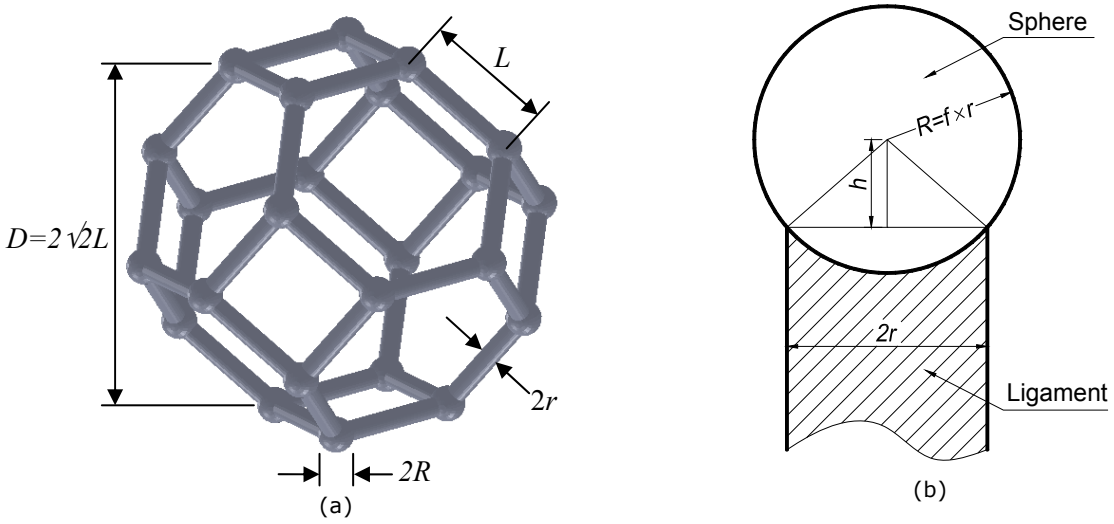

Figure 1: The (a) tetrakaidecahedron with ligaments of (b) circular cross-section shape and spherical nodes at their intersections, is proposed as an example of idealized periodic unit-cell for identification of open-cell foams average characteristic lengths

The second parameter which is widely used to characterize the macroscopic geometry of porous media, and thus polyhedron packing, is the specific surface area S_p, defined as the total solid surface area per unit volume. The hydraulic radius is defined as twice the ratio of the total pore volume to its surface area. This quantity is generally referred to as the thermal characteristic length Λ' in the context of sound absorbing materials [12], such that $\Lambda' = 2\Phi/S_p$. As for the porosity, the thermal characteristic length might be expressed in terms of the microstructural parameters,

$$\Lambda' = \left[\frac{16\sqrt{2}/\left(\frac{2r}{L}\right)^3 - 6\pi/\left(\frac{2r}{L}\right) - 2\pi D_1}{3\pi D_2 + 3\pi\left(2/\frac{2r}{L} - D_3\right)} \right] \times r, \qquad (2)$$

with $D_2 = f^2 - 2f(f - \sqrt{f^2-1})$ and $D_3 = 2\sqrt{f^2-1}$. Above equations are linking micro to macro geometric parameters assuming a tetrakaidecahedron unit-cell with circular cross-section shapes and spherical nodes at their intersections.

When laboratory measurements of porosity and specific surface area (or thermal characteristic length) are available, average ligaments length and thickness can be identified through equations (1) and (2). For instance, we seek for the solution of a cubic equation (1) in r/L that has only one acceptable solution. Once r/L is obtained by assuming a value for f, Eq. (2) gives r. With this relations and laboratory measurements of Φ and S_p, the idealized geometry of the foam can be completely defined.

Foams	Method	Φ (-)	Λ' (μm)	k_0 (m^2)	α_0	Λ (μm)	α_∞	k_0' (m^2)	α_0'
R_1	Computations	0.98	499	2.57×10^{-9}	1.23	291	1.02	50.7×10^{-10}	1.13
	Measurements		440	2.60×10^{-9}		129	1.12	83.0×10^{-10}	
R_{23}	Computations	0.97	478	3.01×10^{-9}	1.26	278	1.02	59.0×10^{-10}	1.14
	Measurements		330	2.98×10^{-9}		118	1.13	97.0×10^{-10}	
R_4	Computations	0.98	645	4.26×10^{-9}	1.22	377	1.01	81.6×10^{-10}	1.14
	Measurements		594	4.24×10^{-9}		226	1.06	131×10^{-10}	

Table 1: Macroscopic geometric and transport parameters of real foam samples.

The main problem in this analysis is that the specific surface area evaluation from non-acoustical measurements, such as the standard Brunauer, Emmett, and Teller method (BET) [13] [14] based on surface chemistry principles, is not routinely available. In fact, the most widely measured parameter after the porosity to characterize the physical macro-behavior of real porous media is unarguably the hydraulic permeability, a quantity having units of length squared and obtainable from the Stokes equations. Making use of this property, it is therefore possible to determine from one numerical test with constant porosity, local characteristic lengths of a tetrakaidecahedron unit cell, as an attempt to grasp quantitatively the complex internal structure of real foam samples. Indeed, the permeability obtained from a computational implementation of the incompressible fluid equations can be displayed as a function of the thermal length squared for a given porosity, showing a linear relation. The quantity that is calculated upon numerical calibration is the slope S to be fitted with the $k_0 = \Lambda'^2$ linear relation. The geometrical property that is extracted is the thermal length Λ' corresponding to the measured static viscous permeability k_0. Making use of Eqs. (1) and (2), local characteristic lengths follows. Hence, there are *a priori* two routinely available independent measurements to be carried out in order to define the foam geometry: the porosity Φ and the static viscous permeability k_0. This method for periodic unit-cell reconstruction circumvents the necessary measure of the specific surface area.

It was then shown how the long-wavelengths acoustic properties of rigid porous media can be numerically determined by solving the local equations governing the asymptotic frequency-dependent dissipation phenomena in a periodic unit cell with the adequate boundary conditions. A detailed presentation of this type of derivation can be found in Ref. [15]. It is assumed that $\lambda >> D$, where λ is the wavelength of an incident acoustic plane wave. This means that for characteristic lengths on the order of $D \sim 0.5$ mm, this assumption is valid for frequencies reaching up to 6000 - 7000 Hz. The asymptotic macroscopic properties of sound absorbing materials are computed from the numerical solution of the incompressible fluid equations (the static viscous permeability k_0, and the static viscous tortuosity α_0), from Laplace equation (the high-frequency tortuosity α_∞, and Johnson's velocity weighted length's parameter Λ), and from the heat equation (the static thermal permeability k_0', and the static thermal tortuosity α_0'). The dynamic viscous (respectively thermal) permeability $\Pi_v(\omega)$ (respectively $\Pi_t(\omega)$) is then derived from successive improvements (see Ref. [16], and [17]-[18] respectively) of the model of Johnson et al. [1] (respectively Champoux and Allard [12],[3]) from which all the pertaining acoustic indicators such as the normal sound absorption coefficient $\alpha(\omega)$ can be deduced, and compared with standing wave tube measurements using an adapted experimental setup [19]. In the following, the 5 parameters (Φ, k_0, α_∞, Λ, Λ') model is referred to Johnson-Champoux-Allard (JCA) simplified model. When k_0' is explicitly taken into account, this is the 6 parameters Johnson-Champoux-Allard-Lafarge (JCAL) model. The complete model relies on 8 parameters (Φ, k_0, k_0', α_∞, Λ, Λ', α_0, and α_0') and is referred to the refined Johnson-Champoux-Allard-Pride-Lafarge (JCAPL) model.

3 Multi-scale results for generated unit-cells and comparison with real foam sample measurements

In order to evaluate our multi-scale methodology, experimental data from microscopy and standing wave tube measurements were used for three real foam samples, R_1, R_{23}, and R_4.

The porosity was non-destructively measured from the perfect gas law properties using the method described by Beranek [20]. The experimental value of the static permeability k_0 was obtained by means of accurate measurements of differential pressures across serial mounted calibrated and unknown flow resistances, with a controlled steady and non-pulsating laminar volumetric air flow as described by Stinson and Daigle [21]. Starting from Φ and k_0 measurements, f was set to 1.5 and average ligaments length L and thickness $2r$ where estimated from the original procedure described in Sec. 2.

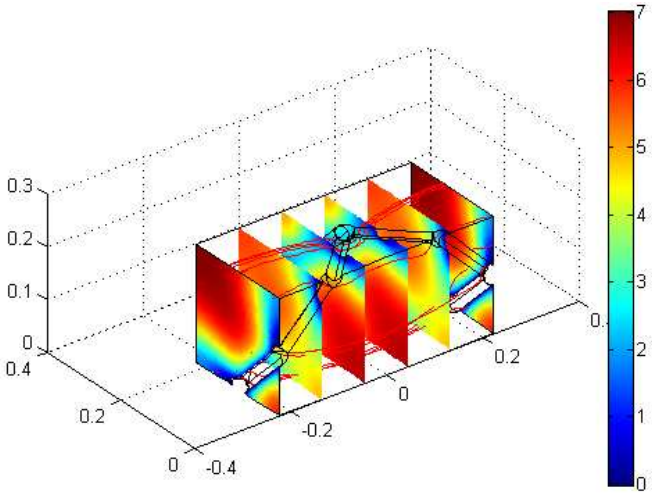

(a)

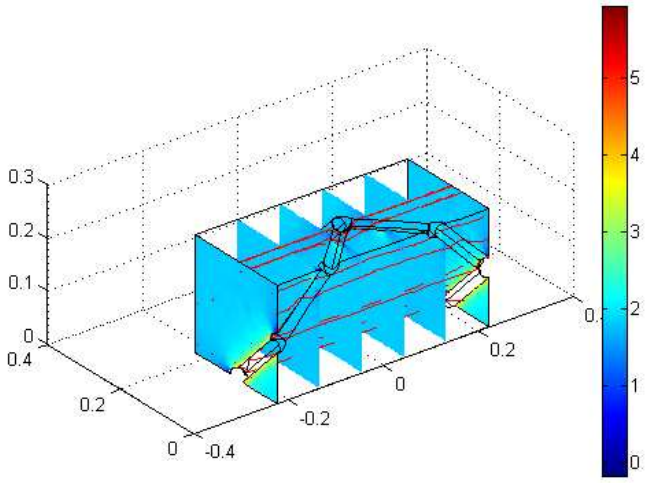

(b)

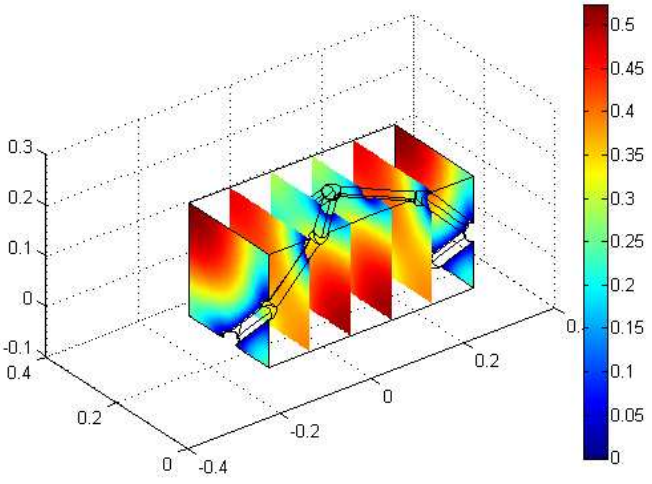

(c)

Figure 2: Asymptotic fields for 1/4th of the reconstructed foam sample period R_4: (a) low-frequency scaled velocity field [$\times 10^{-9}$ m^2], (b) high-frequency scaled velocity field [$\times 10^{-11}$ m^2], and (c) low-frequency acoustic temperature field [° K].

Direct numerical computations of the complete set of macroscopic parameters were performed in reconstructed unit cells (Tab. 1) from adequate asymptotic field averaging (shown in Fig. 2 for foam sample R_1). $\Pi_v(\omega)$, $\Pi_t(\omega)$, and $\alpha(\omega)$ are then analytically derived for JCA, JCAL, and JCAPL models as described in Sec. 2. and compared with standing wave tube measurements, see Fig. 3. Experimental data were provided using the impedance tube technique by Utsuno *et al.* [19], in which the complex and frequency-dependant characteristic impedance $Z_c(\omega)$ and propagation constant $q(\omega)$ of each material were measured, and the equivalent dynamic viscous permeability $\Pi_v(\omega)$, the equivalent dynamic thermal permeability $\Pi_t(\omega)$, and the sound absorption coefficient at normal incidence $\alpha(\omega)$, derived from $Z_c(\omega)$ and $q(\omega)$. In parallel, the material acoustic parameters of the JCAL model were characterized using the method described in Ref. [22] for viscous dissipation and Ref. [23] for thermal dissipation. The computed and characterized viscous (respectively thermal) transition frequencies between viscous and inertial regimes (respectively isothermal and adiabatic), $f_v = \nu\Phi / 2\pi k_0\alpha_\infty$ where ν is the air cinematic viscosity ($f_t = \nu'\Phi / 2\pi k_0\alpha_\infty$ where ν' is the air thermal diffusivity [$m^2.s^{-1}$]) - are also given.

Despite the simplicity of the local geometry model used to study the multi-scale acoustic properties of real foam samples predominately open-celled, there is a relatively good agreement between computed (present microstructural method), measured (impedance tube measurements), and characterized dynamic quantities: $\Pi_v(\omega)$, $\Pi_t(\omega)$, and $\alpha(\omega)$ (see Fig. 3). Furthermore, the general trend given in term of normal incidence sound absorption coefficient $\alpha(\omega)$ by our microstructural approach appears as being particularly relevant, if we notice that it requires only Φ and k_0 as input parameters, and proceed without any adjustable parameter. Discrepancies between measured and computed $\alpha(\omega)$ can be primarily explained from the examination of Λ and α_∞ results reported in Tab. 1. Simulations systematically overestimate Λ with a factor ranging between 1.7 and 2.4, and underestimate α_∞. This means that the windows size of the local geometry model, which respectively plays the role of weighting the velocity field for Λ and rapid section changing for α_∞ by their small openings (the squares and hexagons in the case of a tetrakaidecahedron unit cell), is presumably overestimated by a monodisperse and membrane-free local geometry model.

A further examination of the limits of the micro-cellular model is provided through micrographs. Ligaments lengths were measured on optical micrographs on the real foam samples R_1, R_{23}, and R_4. Foam samples were cut perpendicular to the plane of the sheet. The surface contains exposed cells whose ligament lengths are to be measured on micrographs obtained by light microscopy, Fig 4. Great care was taken during measurements to select only ligaments lying in the plane of observation. Assuming transverse isotropy of the real foam samples, measurements were taken on three-perpendicular planes, and their distributions plotted in Fig. 5.

- For foam sample R_1, membranes are observed on the micrographs. To reach the permeability of the real foam sample exhibiting membranes, the characteristic size of the membrane-free local geometry model must be considerably smaller than the real foam sample, as observed on the ligaments length distribution.
- For foam sample R_{23}, no membranes were observed on the micrographs. However, the characteristic size of the local geometry model corresponds to the left-peak of a bimodal distribution, which governs the overall permeability of the real foam sample (this is the critical-path argument; see Ref. [9] - Sec. V).
- For foam sample R_4, neither membrane nor distinctive bi-modal ligaments distribution was observed. The ligaments length of the local geometry model is close to the averaged value measured on the micrographs (especially for the horizontal surface, through which permeability measurements were performed). And the ligament length found by inversion is in good agreement with averaged measured characteristic lengths of the real open-celled foam sample.

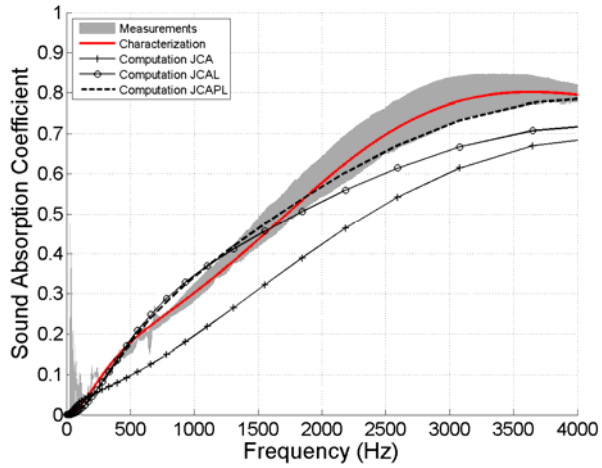

(a)

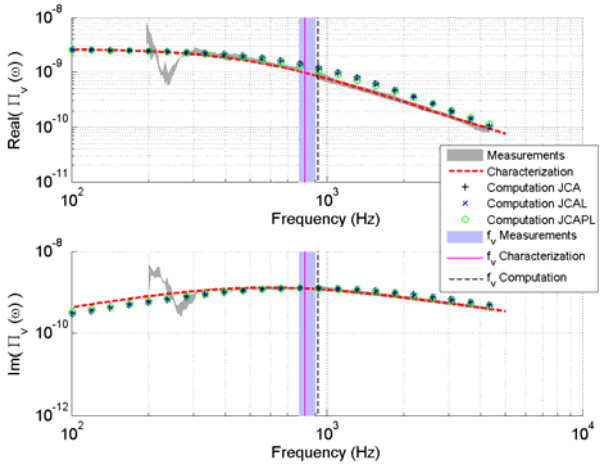

(b)

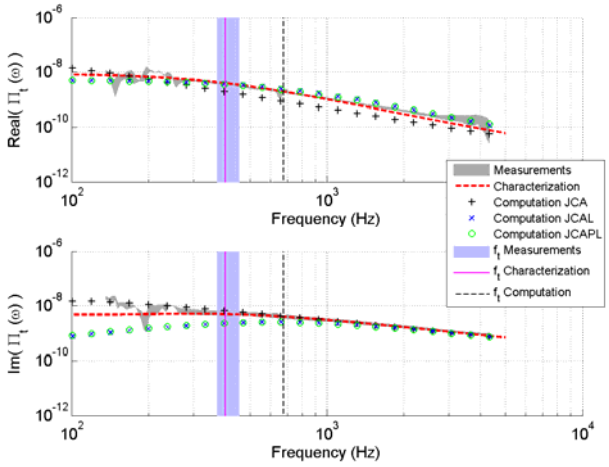

(c)

Figure 3(A): (a) Normal incidence sound absorption coefficient α(ω), (b) dynamic viscous permeability $\Pi_v(\omega)$, and (c) dynamic thermal permeability $\Pi_t(\omega)$ for foam sample R_1: Comparison between measurements, characterization, and computations.

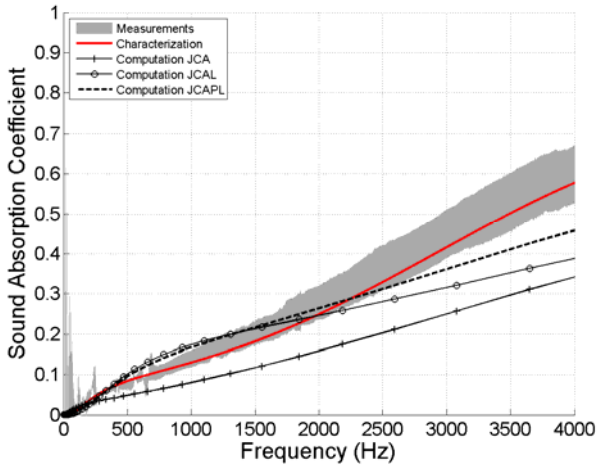

(a)

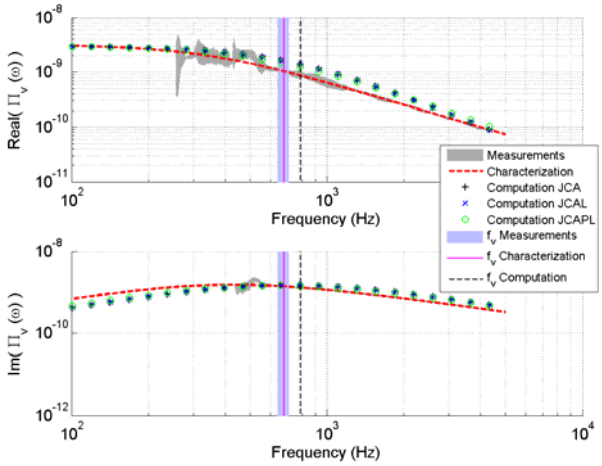

(b)

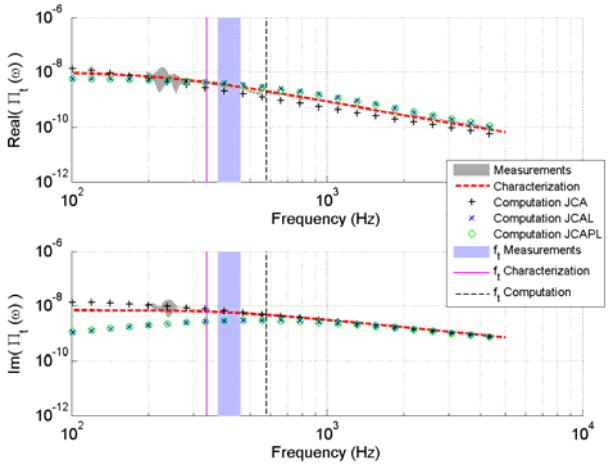

(c)

Figure 4(B): (a) Normal incidence sound absorption coefficient α(ω), (b) dynamic viscous permeability $\Pi_v(\omega)$, and (c) dynamic thermal permeability $\Pi_t(\omega)$ for foam sample R_{23}: Comparison between measurements, characterization, and computations.

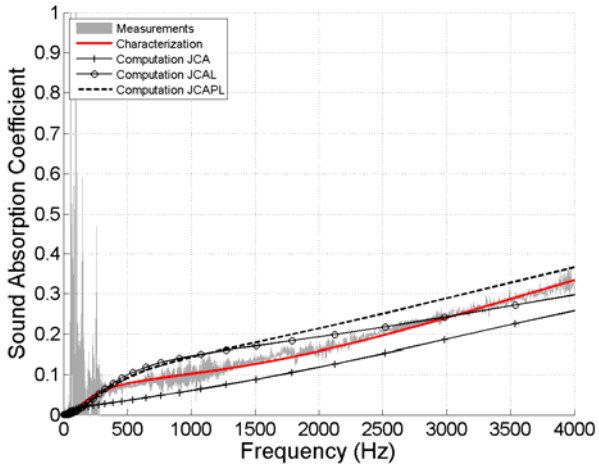

(a)

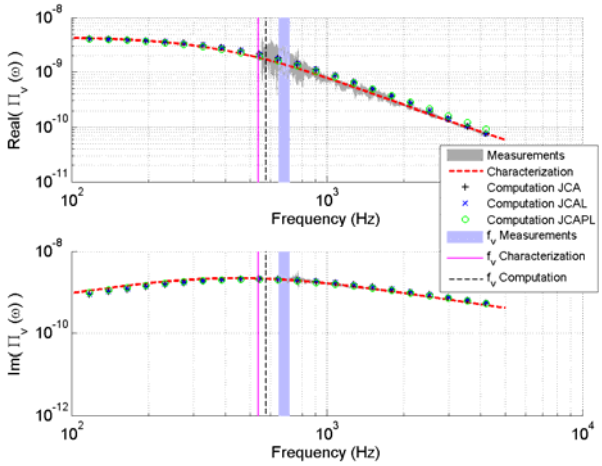

(b)

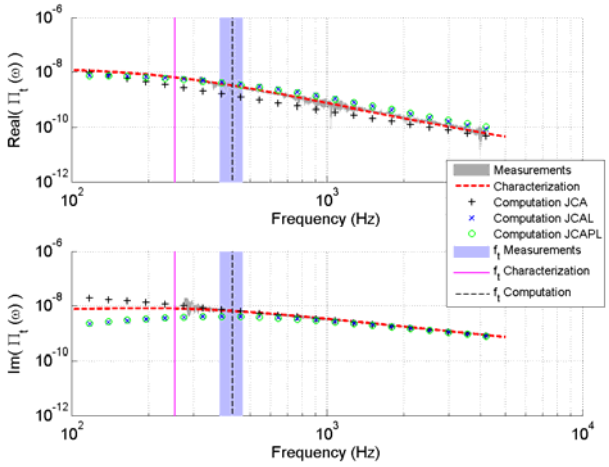

(c)

Figure 5(C): (a) Normal incidence sound absorption coefficient α(ω), (b) dynamic viscous permeability $\Pi_v(\omega)$, and (c) dynamic thermal permeability $\Pi_t(\omega)$ for foam sample R_4: Comparison between measurements, characterization, and computations.

(a)

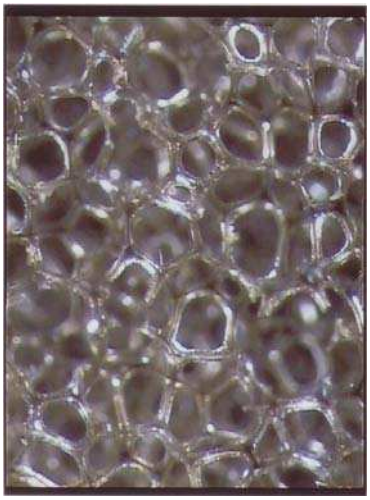

(b)

(c)

Figure 4: Micrographs obtained by optical microscopy of real foam samples (a) R_1, (b) R_{23}, and (c) R_4 [Scale: Each micrograph is 1187.5 µm in width].

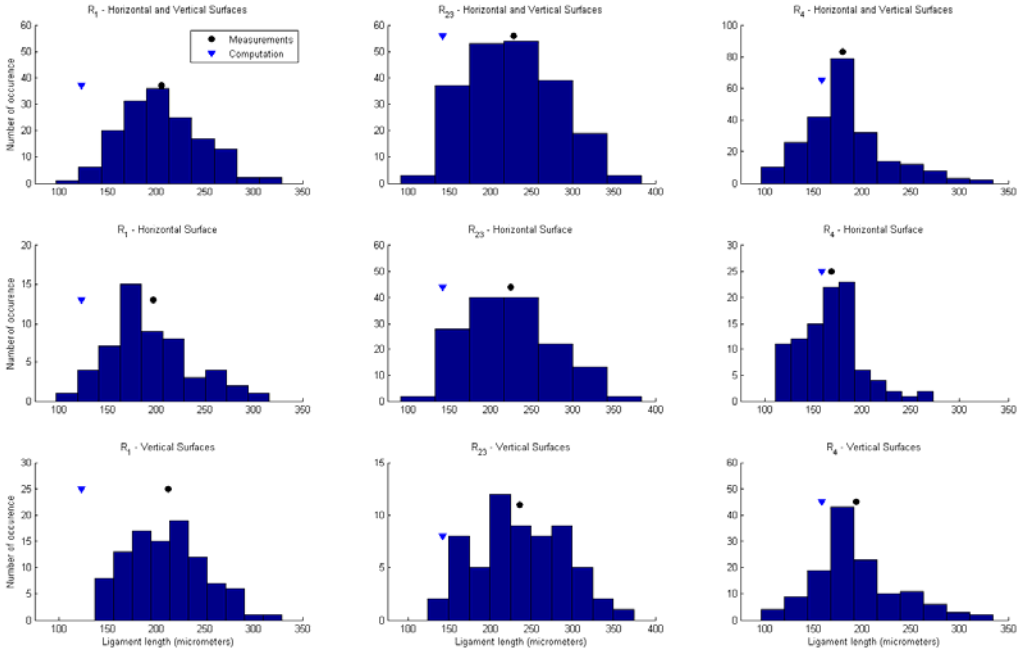

Figure 5: Ligament length distributions for real foam samples (left) R_1, (center) R_{23}, and (right) R_4. In the legend, Measurements (●) accounts for ligaments lengths characterizations through micrographs, whereas (▼) Computation stands for ligaments length of the tetrakaidecahedron unit-cell used for numerical simulations.

4 Conclusions

A three-dimensional idealized periodic unit-cell (PUC) based method to obtain the acoustic properties of three predominately open-celled foam samples was described. The first step was to provide the local characteristic lengths of the representative unit cell. For isotropic open cell foams, two input parameters were required, the porosity and the hydraulic permeability. Long wavelengths acoustic properties were derived from the three-dimensional reconstructed PUC by solving the boundary value problems governing the micro-scale propagation and visco-thermal dissipation phenomena with adequate periodic boundary conditions, and further field phase averaging. The computed acoustic properties of the foams were found to be in relatively good agreement with standing wave tube measurements. A close examination of the real foam samples ligaments length distribution as observed from micrographs, and its comparison with the characteristic size of the local geometry model, showed evidences of membrane and bimodal pore-size distribution effects. The overall picture that emerges from that work is that the acoustical response of these materials is governed by their three-dimensional micro-cellular morphology, for which an idealized unit-cell based method is a convenient framework of multi-scale analysis displaying the microgeometry features having a significant impact on the overall response function of the porous media.

References

[1] J. W. S. Rayleigh, *The theory of sound*, 2nd Ed., Dover, New York (1945).

[2] C. Zwikker and C. W. Kosten, Sound absorbing materials, Elsevier, Amsterdam (1949).

[3] J. F. Allard and N. Atalla, *Propagation of Sound in Porous Media: modeling sound absorbing materials*, 2nd Ed., Wiley, Chichester (2009).

[4] L. J. Gibson, M. F. Ashby, *Cellular solids: Structure and Properties*, Cambridge University Press, Cambridge (1988).

[5] D. Weaire, S. Hutzler, *The Physics of Foams*, Oxford University Press, Oxford (1999).

[6] D. L. Johnson, J. Koplik, R. Dashen, *Theory of dynamic permeability and tortuosity in fluid-saturated porous media*, J. Fluid Mech. Vol. 176 (1987), pp. 379-402.

[7] M. R. Stinson, *The propagation of plane sound waves in narrow and wide circular tubes, and generalization to uniform tubes of arbitrary cross-sectional shape*, J. Acoust. Soc. Am. 89 (1991), pp. 550-558.

[8] C. Boutin, C. Geindreau, *Estimates and bounds of dynamic permeability of granular media*, J. Acoust. Soc. Am. Vol. 124 (2008), pp. 3576–3593.

[9] M. Y. Zhou, P. Sheng, *First-principles calculations of dynamic permeability in porous media*, Phys. Rev. B 39 (1989), pp. 12027-12039.

[10] P. M. Adler*, Porous Media: Geometry and Transports, Butterworth-Heinemann*, Stoneham (1992).

[11] E. N. Schmierer, A. Razani, J. W. Paquette, and K. J. Kim, *Effective Thermal Conductivity of Fully Saturated High Porosity Foam*, Proceedings of 2004 ASME Heat Transfer/Fluids Engineering Summer Conference (2004), pp. 229-237.

[12] Y. Champoux, J. F. Allard, *Dynamic tortuosity and bulk modulus in air-saturated porous media*, J. Appl. Phys. Vol. 70 (1991), pp. 1975-1979.

[13] S. Brunauer, P. H. Emmett, E. Teller, *Adsorption of Gases in Multimolecular Layers*, J. Am. Chem. Soc., Vol. 60 (1938), pp 309–319.

[14] M. Henry, P. Lemarinier, J. F. Allard, J. L. Bonardet, A. Gedeon, *Evaluation of the characteristic dimensions for porous sound-absorbing materials*, J. Appl. Phys. Vol. 77 (1994), pp. 17-20.

[15] C. Perrot, F. Chevillotte, R. Panneton, *Bottom-up approach for microstructure optimization of sound absorbing materials*, J. Acoust. Soc. Am. Vol. 124 (2008), pp. 940-948.

[16] S. R. Pride, F. D. Morgan, and A. F. Gangi, *Drag forces of porous media acoustics*, Phys. Rev. B 47, (1993) pp. 4964-4975.

[17] D. Lafarge, *Propagation du son dans les matériaux poreux à structure rigide saturés par un fluide viscothermique*, Ph. D. Thesis, Université du Maine, 1993; translation in English : *Sound propagation in rigid porous media saturated by a viscothermal fluid*".

[18] D. Lafarge, P. Lemarinier, J. F. Allard, V. Tarnow, *Dynamic compressibility of air in porous structures at audible frequencies*, J. Acoust. Soc. Am. Vol. 102 (1997), pp. 1995-2006.

[19] H .Utsuno, T. Tanaka, T. Fujikawa, A. F. Seybert, *Transfer function method for measuring characteristic impedance and propagation constant of porous materials*, J. Acoust. Soc. Am. Vol. 86 (1989), pp. 637.

[20] L. L. Beranek, *Acoustic impedance of porous materials*, J. Acoust. Soc. Am. Vol. 13 (1942), pp. 248-260.

[21] M. R. Stinson and G. A. Daigle, *Electronic system for the measurement of flow resistance*, J. Acoust. Soc. Am. Vol. 83 (1988), pp. 2422-2428.

[22] R. Panneton, X. Olny, *Acoustical determination of the parameters governing viscous dissipation in porous media*, J. Acoust. Soc. Am. Vol. 119 (2006), pp. 2027-2040.

[23] X. Olny, R. Panneton, *Acoustical determination of the parameters governing thermal dissipation in porous media*, J. Acoust. Soc. Am. Vol. 123 (2008), pp. 814-824.